JOURNAL OF GEOPHYSICAL RESEARCH, VOL. 114, C05021, doi:10.1029/2008JC005196, 2009

Remote sensing of the Dead Sea surface temperature

R. Nehorai,[1,2] I. M. Lensky,[1] N. G. Lensky,[2] and S. Shiff[1]

Received 13 November 2008; revised 19 February 2009; accepted 18 March 2009; published 28 May 2009.

[1] The Dead Sea is a unique terminal lake located at the lowest place on Earth's surface. It has the highest surface temperature, salinity, and density among Earth's large water bodies, and its level is currently dropping at a rate of ~1 m/a. Knowledge of the Dead Sea thermal and saline structure is based on meteorological and hydrological measurements from a single site at a time. In this study, we used satellite and in situ data to characterize the spatial and temporal variations of the Dead Sea sea surface temperature (SST) and to explore the causes for these variations. Sequences of almost continuous individual satellite images were transformed into a time series of parameters representing the spatial distribution of SST. Also used were in situ measured bulk SST, wind speed, solar radiation, and water temperature profiles with depth. Analysis of this data set shows strong diurnal and seasonal variations of the surface and vertical temperature field and the meteorological forcing. The temperature field is heterogeneous after noon, when radiation is high and wind speed is low and thermal layering develops. The temperature field is homogeneous during the nighttime, when solar radiation is absent and the high wind speed vertically mixes the upper layer.

Citation: Nehorai, R., I. M. Lensky, N. G. Lensky, and S. Shiff (2009), Remote sensing of the Dead Sea surface temperature, J. Geophys. Res., 114, C05021, doi:10.1029/2008JC005196.

1. Introduction

[2] The Dead Sea is a hypersaline terminal lake and is the lowest, hottest, and densest among the large water surfaces on Earth (421 m below sea level, salinity ~277 g/kg, density ~1240 kg/m^3 at 25°C, and surface temperatures ~33–36°C during the summer diurnal cycle, Figure 1a). Its surface area is ~633 km^2, and it has a maximum depth of ~300 m. Because of diversion of fresh water from its drainage basin, the Dead Sea's water balance has been negative in the past decades, and consequently, its level has declined, currently at a rate of ~1 m/a, and its salinity and temperature have risen at a rate of ~0.3 g/kg/a and 0.25°C/a, respectively [Gertman and Hecht, 2002]. The increase of salinity results in a reduced evaporation rate, which in turn results in an increased surface temperature [Lensky et al., 2005]. The summer thermocline is generally located at a depth of between 25 and 30 m with a temperature gradient of >10°C over 5 m. A secondary summer thermocline develops at a depth of a few meters during the daytime with a maximum temperature gradient of 4°C over the top 5 m. Overturn occurs following the autumn cooling of the saltier upper water layer and the consequent increase in its density. The Dead Sea remains vertically mixed during the winter unless unusual amounts of fresh water reach the Dead Sea and dilute the upper water layer in extremely rainy years (e.g., 1991–1992).

[3] The current knowledge of the dynamics of the thermal and salinity structure of the Dead Sea has been achieved primarily from measured vertical profiles of temperatures, salinity, and density (from the surface to the bottom) collected over the past 50 years [Anati, 1997; Beyth et al., 1993; Gavrieli and Oren, 2004; Gertman and Hecht, 2002; Hecht and Gertman, 2003; Ivanov et al., 2002; Neev and Emery, 1967; Stanhill, 1990; Steinhorn and Gat, 1983]. A hydrometeorological buoy was placed in the center of the Dead Sea in 1992, and since then (except for a gap between 2002 and 2004), it has been recording meteorological data over the Dead Sea surface and the temperature profile from the surface down to a depth of 40 m [Gertman and Hecht, 2002; Hecht and Gertman, 2003]. This data set led to the formulation of its mass and energy balances [Lensky et al., 2005; Neumann, 1958; Stanhill, 1985]. However, because of the lack of data on the spatial variations of sea surface temperature (SST), it is unclear to what extent the measured surface temperature in a single location represents the surface temperature of the whole Dead Sea area. Spatial variations of the Dead Sea surface temperature may affect the estimated mass and energy balances of the Dead Sea. In the pioneering study of the Dead Sea SST by Stanhill [1990], lateral temperature variations were detected using thermal survey cruises (profiles) and by means of remote sensing. Since the remote sensing images were received only twice a day and the collection of each profile took several hours, the spatial variations within the diurnal cycle could not be resolved. Recent improvements in the remote sensing technology enabled us to observe the spatial distribution of the Dead Sea SST almost continuously with a spatial resolution of ~4 km.

[1]Department of Geography and Environment, Bar-Ilan University, Ramat-Gan, Israel.
[2]Geological Survey of Israel, Jerusalem, Israel.

0148-0227/09/2008JC005196$09.00

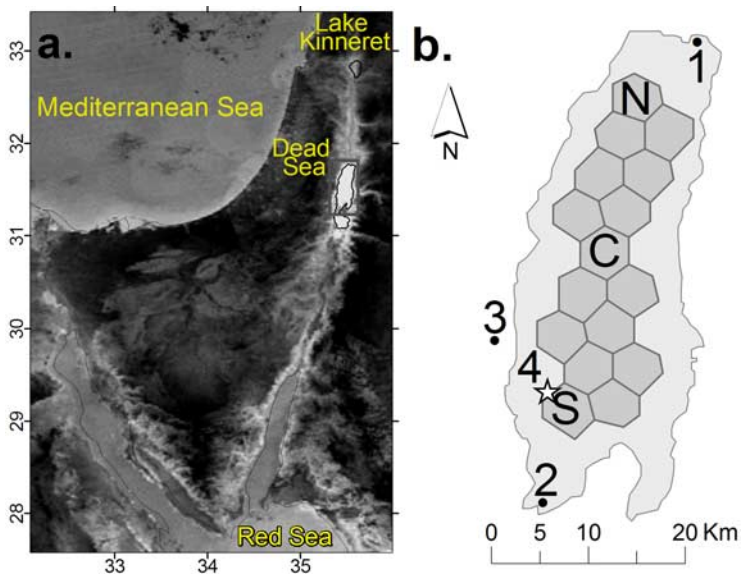

Figure 1. (a) Thermal image of the eastern Mediterranean from Moderate Resolution Imaging Spectroradiometer, 3 August 2005, 1950 UT. Note that the highest surface temperature in the area (brightest pixels) is the Dead Sea surface. (b) Location of 16 MSG pixels (gray polygons). The numbers in the map refer to the following: 1, the Jordan River inlet; 2, the reject brine inlet; 3, En Gedi; 4, the buoy (located at the star). The letters N, C, and S stand for the northern, central, and southern pixels, respectively. The polygons were calculated by the Thiessen polygons method [Thiessen, 1911], which is used to apportion pixel coverage into polygons.

[4] Here we present a method for characterizing spatial and temporal variations in SST, apply it to the Dead Sea, and explore the causes for these variations in terms of meteorological conditions. Special emphasis is placed on the diurnal SST spatial variations and their relation to the dramatic change in the wind and radiation forcing during the 24 h cycle. The data processed in this study facilitate comparisons among diurnal cycles from different seasons.

2. Methods

2.1. Remote Sensing

[5] There is a significant change in the meteorological forcing during the diurnal cycle. Therefore, we sought a response in the SST field to these changes. We used the almost continuous measurements of the Dead Sea brightness temperature at three thermal infrared (IR) (see Table 1 for list of acronyms) window channels of the Spinning Enhanced Visible and Infrared Imager (SEVIRI) on board the Meteosat Second Generation (MSG) (the European geostationary satellite operated by the European Organization for the Exploitation of Meteorological Satellites). The spatial resolution of the MSG images is 3 km at nadir and about 4.3 km at the Dead Sea; the images are collected every 15 min. A complete overview of the MSG SEVIRI instrument is provided by Schmetz et al. [2002]. To extract the brightness temperature from the three thermal IR window channels centered at 8.7, 10.8, and 12 μm, we used the Clouds-Aerosols-Precipitation Satellite Analysis Tool [Lensky and Rosenfeld, 2008]. We used near-IR reflectance at 1.6 μm to delineate only a total of 16 MSG pixels, conservatively selected, that cover the Dead Sea surface and eliminated pixels partly covering land to avoid thermal contamination in the SST retrieval (Figure 1b).

Table 1. Acronyms

Acronym	Term
IR	infrared
MSG	Meteosat Second Generation
SST	sea surface temperature
SST_{buoy}	bulk temperature as measured from the buoy at a 1 m depth
SST_{MSG}	skin SST calculated from the MSG
SST^{ave}_{MSG}	average SST_{MSG} calculated from the 16 MSG pixels
SST^{N}_{MSG}	MSG pixel from the northern Dead Sea
SST^{C}_{MSG}	MSG pixel from the central Dead Sea
SST^{S}_{MSG}	MSG pixel from the southern Dead Sea, collocated with the buoy
ΔSST^{N}	deviation of the northern pixel's SST from the average: $SST^{N}_{MSG} - SST^{ave}_{MSG}$
ΔSST^{C}	deviation of the central pixel's SST from the average: $SST^{C}_{MSG} - SST^{ave}_{MSG}$
ΔSST^{S}	deviation of the southern pixel's SST from the average: $SST^{S}_{MSG} - SST^{ave}_{MSG}$
SD	standard deviation of SST from the MSG temperature calculated from 16 pixels

2.2. In Situ Measurements

[6] We used in situ meteorological and hydrological data to complement the remotely sensed measurements. The data set includes wind speed, solar radiation, and water temperature at depths of 1–40 m (1, 2, 3, 4, 6, 8, 10, 15, 20, 25, 30, and 40 m). These parameters were collected every 20 min at the hydrometeorological buoy, located ~5 km offshore of En Gedi (Figure 1b). The details of the data collection are described by Gertman and Hecht [2002] and Hecht and Gertman [2003]. We used the Dead Sea SST measured at the buoy at 1 m depth (SST_{buoy}) to calibrate the SST retrieved by the satellite (SST_{MSG}). The temperature measured at 1 m represents the bulk temperature of the upper water layer, whereas the temperature measured from the radiometers in the satellite represents the skin layer, which constitutes the upper few microns that interact directly with the atmosphere.

3. Data Processing

3.1. Calibration: Remote Sensing Versus in Situ Measurements

[7] Thermal IR radiation emitted from the Dead Sea surface travels through an additional atmospheric layer of 421 m containing haze particles [Levin et al., 2005] before reaching reference sea level, preventing the use of operational SST algorithms, which are usually calibrated for sea level. Following the usual calibration procedure [Barton, 2001; Emery et al., 2001; Li et al., 2001], we derived the algorithm coefficients by multilinear regression of the three MSG thermal IR window channels against the in situ SST_{buoy}. We used the MSG pixel collocated with the buoy ("S" in Figure 1b) for the calibration. Over a thousand 15-min interval MSG images were collected between 27 July 2005 (1500 UT) and 8 August 2005 (1500 UT). In four of these summer observation days we detected the Mediterranean Sea breeze front [Alpert and Rabinovich-Hadar, 2003] using the "desert dust" color scheme [Lensky and Rosenfeld, 2008]. In those 4 days, shortly after the temperature reached its maximum, we detected a steep decline in the skin SST (SST^{S}_{MSG} and SST^{ave}_{MSG}) but not in the bulk SST. The drop in the skin SST is an artifact attributed to absorption of thermal IR radiation by water vapor in the atmosphere. This is supported by the observation of a slight drop in the solar radiation in three of those days, revealing that some of the water vapor condensed (reflecting some of the short-wave solar radiation back to space). The screening of the Dead Sea surface by the sea breeze front mandated exclusion of these data from this study.

[8] For validation we used another data set of 191 MSG images for the period between 11 August 2005 (1515 UT) and 13 August 2005 (1500 UT). A linear regression between SST_{MSG} and SST_{buoy} showed a coefficient of determination $r^2 = 0.8$. To explore the seasonal variations of SST, we studied 2-day periods in the summer, autumn, and winter.

3.2. From SST Images to a Time Series

[9] We looked for time series of significant statistical quantities representing the spatial distribution of the SST over the Dead Sea. Here we describe a four-step procedure for transforming a sequence of individual MSG images into a time series: (1) storing the SST data at each time step (each image consists of 16 pixels); (2) calculating the average SST of all pixels in each image (SST^{ave}_{MSG}), the standard deviation (SD) of SST of all pixels in each image, and the deviation of the northern, central, and southern pixels (SST^{N}_{MSG}, SST^{C}_{MSG}, and SST^{S}_{MSG}) from the average SST (ΔSST^{N}, ΔSST^{C}, and ΔSST^{S}); (3) presenting a time series of SST^{ave}_{MSG}, SD, and ΔSST^{N}, ΔSST^{C}, and ΔSST^{S}; and (4) presenting a time series of in situ measured bulk SST (SST_{buoy}), wind speed, and solar radiation.

4. Data Analysis

4.1. Diurnal Cycle of the SST Spatial Distribution and the Meteorological Forcing

[10] Figure 2 presents the strong diurnal variations of the SST field and the meteorological forcing on the SST on a typical summer day (5 August 2005). Figure 2 includes a time series of the following: bulk SST (SST_{buoy}), skin SST (SST^{S}_{MSG} and SST^{ave}_{MSG} in Figure 2a), spatial variations of SST in two forms (ΔSST^{N}, ΔSST^{C}, ΔSST^{S} in Figure 2b and SD in Figure 2c), and the meteorological forcing (wind speed and solar radiation in Figure 2d).

[11] There is a good match between the three series in Figure 2a showing the diurnal cycle with an amplitude of 2°C and minimum SST of 33°C at nighttime, similar to the well-described Dead Sea diurnal cycle from the buoy data [Gertman and Hecht, 2002; Hecht and Gertman, 2003]. The bulk SST is much smoother than the skin SST time series (typical oscillation amplitude ~0.2–0.3°C). This is attributed to the higher thermal inertia of the bulk upper water layer compared to the molecular-scale skin layer which quickly builds and breaks up [Wick et al., 1996]. About 1 h after sunrise, the skin SST (SST^{S}_{MSG} and SST^{ave}_{MSG}) starts to rise, preceding the bulk SST (SST_{bouy}) by 2 h. SST reaches its maximum about 2 h after maximum radiation, where the maximum skin SST precedes the bulk by about 1 h.

[12] The diurnal cycle of the spatial variations of the Dead Sea SST is presented in Figures 2b and 2c. Figure 2b shows that during daytime the differences among the SST of the northern, central, and southern pixels and the SST^{ave}_{MSG} are significantly higher than during nighttime. During daytime the southern pixel is usually warmer than the average Dead Sea surface (positive ΔSST^{S}), whereas the central and northern pixels are usually cooler (negative ΔSST^{C} and ΔSST^{N}). At nighttime the spatial pattern is less pronounced, with smaller differences. Similarly, Figure 2c presents the degree of SST heterogeneity in terms of SD of SST. Heterogeneous distribution of SST (high SD) is limited to low wind speed (<5 m/s) and to high radiation. Homogeneous SST (low SD) is related to low radiation and high wind speed (mostly during nighttime).

[13] The SST heterogeneity is affected by the wind speed and solar radiation (Figures 2c and 2d). These force the system by introducing radiative heat and mechanical energy. The wind speed is low (<5 m/s) during daytime and high (>5 m/s) during nighttime. The transition from the tranquil day winds to the stronger night winds occurs around sunset (±1 h) as the Mediterranean Sea breeze passes over the Dead Sea from north to south. The SST heterogeneity is maximal a couple of hours after the maximum solar

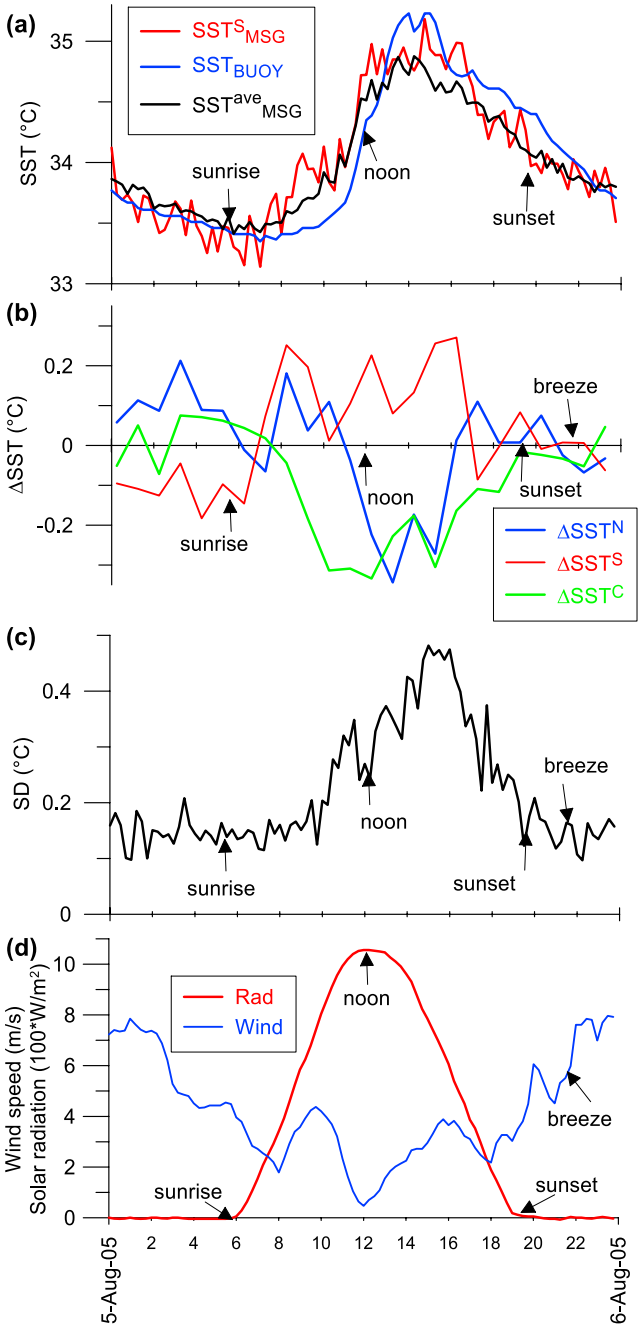

Figure 2. Diurnal cycle of (a) SST; (b) the deviation of the northern, central, and southern pixels from the average; (c) the standard deviation of SST; and (d) the wind speed and solar radiation.

radiation (SD $\sim$ 0.6°C) and minimal during nighttime ($\sim$0.2°C). High SD is limited to low wind speed (<5 m/s) and to high radiation. Low SD is related to low radiation (mostly during nighttime).

[14] In order to check to what extent the results shown in Figure 2 represent a typical diurnal cycle, we cross correlated pairs of these parameters over a period of 10 days. In Figure 3 the x axis is the shift in hours between the two parameters, and the y axis is the correlation for each of these pairs. For example, the shape of the time series curves of SST (Figure 2a) and the solar radiation (Figure 2d) along the diurnal cycle is very similar except that SST lags behind the radiation. This is shown in Figure 3, where a correlation of 0.66 is achieved with a 2.75 h shift. Similarly, the cross correlation between the SD and the wind speed shows a negative correlation of -0.46 at a shift of 1.75 h. The cross correlation between the bulk and skin SST shows a correlation of 0.87 at a 0.75 h shift. This lag reflects the smaller thermal inertia of the thin skin compared to the bulk. These cross correlations and others (not shown in Figure 3) are summarized in Table 2.

4.2. Seasonal Variations

[15] Figure 4 presents the seasonal changes of the diurnal cycle of SST and the meteorological forcing. The SD shows a similar diurnal cycle with its maximum after noon in all seasons but with different amplitudes, the highest occurring in the summer (0.6°C) and the lowest occurring in the winter (0.15°C), with intermediate values in autumn (Figure 4a). In all seasons the southern part of the Dead Sea is warmer than the northern part during daytime (Figure 4b). The maximum solar radiation decreases from 1150 W/m^2 in summer to 850 W/m^2 in winter, with intermediate values in autumn (Figure 4c). The maximum daily spatial variation decreases with the seasonal decrease of maximum solar radiation. The wind speed is generally high in nighttime and low in daytime in all seasons.

5. Discussion and Summary

[16] In this study we characterized the spatial and temporal variations of the Dead Sea surface temperature and explored the causes for these variations in terms of meteorological conditions. Special emphasis was put on the spatial variations in the diurnal cycle at the different seasons. We developed a four-step procedure transforming sequences of individual MSG images and in situ measurements into a time series. The time series included the average and the standard deviation of SST, the deviation of different pixels from the average (northern, central, and southern), bulk SST (1 m depth), wind speed, and solar radiation.

5.1. Surface and Vertical Temperature Heterogeneity and the Meteorological Forcing

[17] We presented strong diurnal variations of the SST field and its relation to the diurnal meteorological forcing. High values of SD, indicating heterogeneous SST, are related to lower wind speed (<5 m/s) and higher radiation. Low SD is related to low radiation (mostly during the nighttime) and is usually related to high wind speed. Viewing the vertical temperature variations with time provides complementary information, which is necessary for the understanding of the three-dimensional thermal structure and the meteorological forcing. Figure 5 presents the time series of the meteorological forcing and the SST heterogeneity (SD) together with the vertical temperature structure of the upper water layer collected from the buoy. Here we focus on the daily upper layer, with a typical depth of $\sim$5 m, which builds up during the daytime and is destroyed during the nighttime. The seasonal layering includes an upper layer of 20–30 m, which builds up during the summer and is destroyed during the winter, resulting in a fully mixed lake.

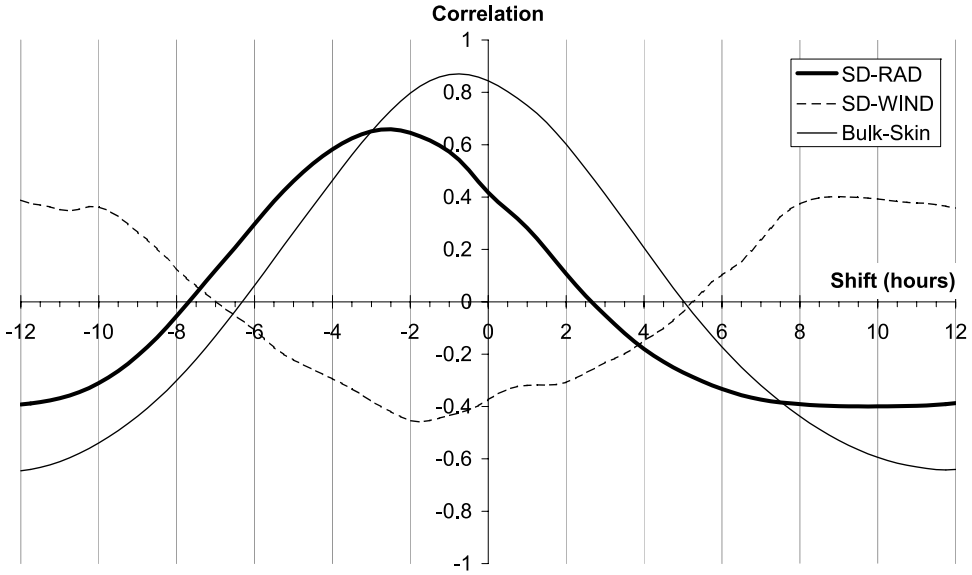

Figure 3. Cross correlation between the following pairs: SD of SST and the solar radiation (RAD), SD and the wind speed (WIND), and bulk and skin SST.

Figure 5 shows the relation of the buildup of the upper warmer layer during daytime (Figure 5c) to the buildup of SST variations (Figure 5b), which are both generated by the solar radiation heating (Figure 5a). In the evening, after sunset and with the arrival of the Mediterranean Sea breeze, the upper warm layer mixes with the lower and cooler water because of the wind action (Figures 5a and 5c). This results in a homogeneous upper water layer and homogeneous surface temperature (i.e., vertical and horizontal homogeneity). In the morning, as the wind speed decreases and the solar radiation increases, the uppermost layer builds up again, and a new diurnal cycle begins. Since the incoming solar radiation is practically uniform (mostly clear sky), the high lateral SST variation associated with high radiation cannot be attributed to spatial variations in the incoming radiation. We thus suggest that when the upper water is well mixed during the nighttime, the surface temperature is more homogeneous across the sea surface. During the daytime, a vertical thermal layer develops on a meter scale (Figure 5c) and on a micron scale (skin layer). Such a structure is very fragile, and local winds can easily break it [Wick et al., 1996] and cause the observed spatial SST variations.

[18] It should be noted that the strong winds during the nighttime (5–10 m/s) are expected to cause vertical mixing (section 5.1) and horizontal currents. The two phenomena have opposite consequences in terms of SST; the vertical mixing is expected to homogenize the SST, whereas horizontal currents are expected to result in a heterogeneous temperature distribution, as was observed at Lake Tahoe [Steissberg et al., 2005]. Our results suggest that in the Dead Sea the major impact of the wind is the homogenization of the upper mixed layer. Thus, it seems that the SST spatial patterns in the Dead Sea are related more to the buildup and breakup of the thermal layer than to horizontal currents.

5.2. Spatial Variation and Its Influence on Evaporation

[19] The daytime deviation of the SST northern, central, and southern pixels from the average is significantly higher than during the nighttime. The southern pixel (collocated with the buoy) is warmer by 0.2–0.4°C at noon and cooler by 0.1–0.2°C at nighttime, revealing the extent to which the SST measured by the buoy represents the Dead Sea SST. The average difference between the buoy and the average temperature of the Dead Sea is ~0.05°C. As a consequence, the evaporation calculated using buoy data [Lensky et al., 2005] requires correction for this slight difference. Using the energy balance approach (following the procedure of Lensky et al. [2005]), such a difference results in a higher evaporation rate for the entire Dead Sea surface by ~0.5% or on an annual basis by about 0.5 cm/a, which translates to $\sim 3 \times 10^6$ m^3/a of evaporated water. The observation that the SST in the southern part of the Dead Sea is usually higher than average during the daytime may be explained by the more arid conditions in the southern Dead Sea compared to its northern part, as reported by Alpert et al. [1997]; however, this should be studied further.

5.3. Seasonal Variations

[20] The seasonal variations of the diurnal cycle of SST are generally similar in the different seasons, with larger amplitudes of spatial variations and with increasing solar radiation. The maximum standard deviation of SST appears after noon in all seasons but varies in amplitude; it is the highest in the summer and gradually decreases toward the

Table 2. Cross Correlation Between Pairs of Parameters[a]

Correlation Pairs	Lag (h)	Correlation
SST_{buoy}-SST^{S}_{MSG} (bulk-skin)	−0.75	+0.87
SST_{buoy}-SD	0	+0.57
SST_{buoy}-radiation	−3.5	+0.88
SST_{MSG}^{S}-radiation	−2.5	+0.87
SD-radiation	−2.5	+0.66
SST_{buoy}-wind	−2	−0.76
SST_{MSG}^{S}-wind	−1.75	−0.59
SD-wind	−1.75	−0.46

[a]See Figure 3.

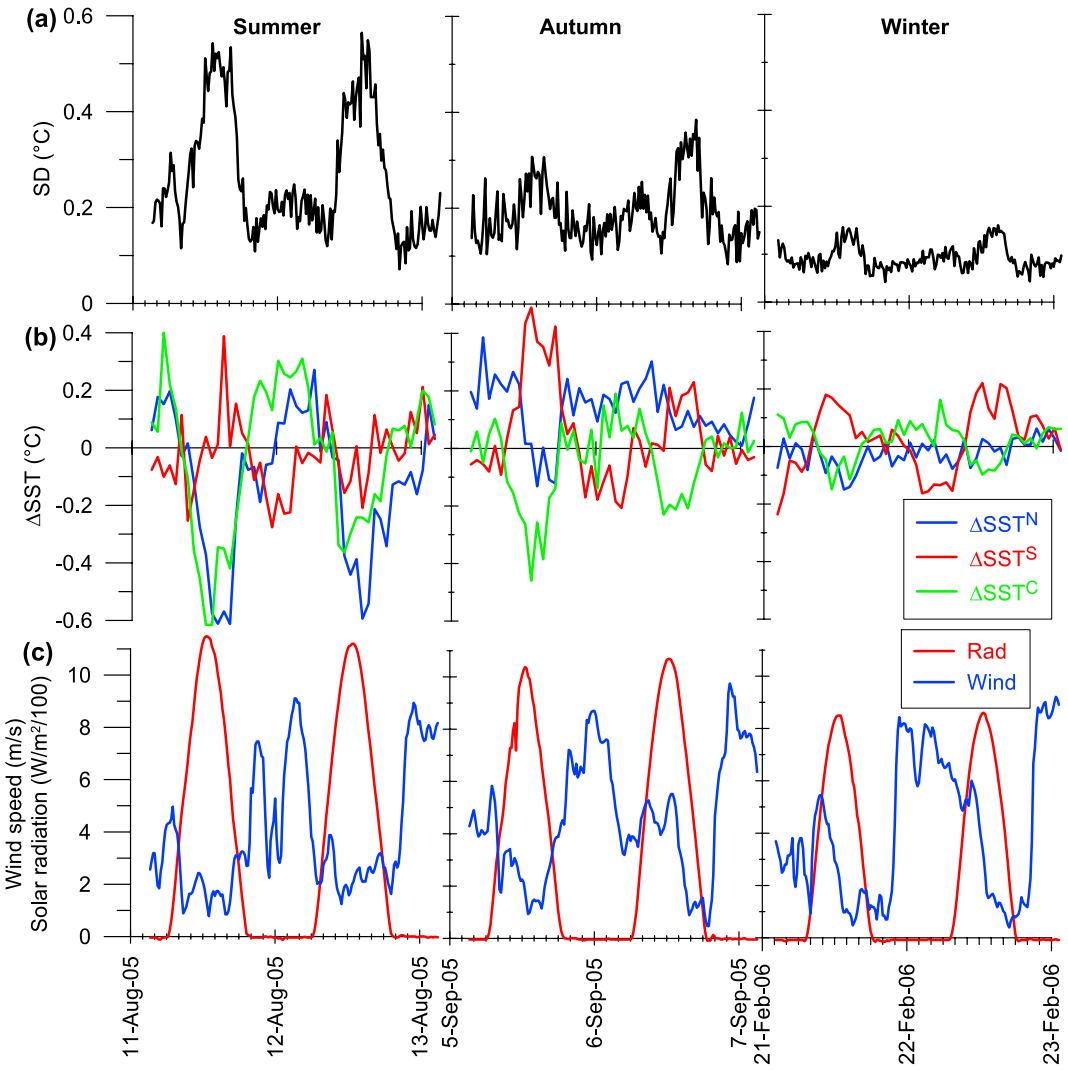

Figure 4. Seasonal variations of the diurnal cycle. The spatial variations of SST: (a) the standard deviation of SST and (b) deviation of the northern, central, and southern pixels from the average. (c) The wind speed and solar radiation.

winter. It seems that the seasonal variations in the SST patterns are governed by the intensity of incoming solar radiation; the wind speed does not change significantly during the seasonal cycle. As the solar radiation decreases toward the winter, the vertical temperature gradient decreases, and as a result the surface temperature variations decrease. In all seasons the southern part of the Dead Sea is warmer during the daytime than the northern part.

[21] The buildup and destruction of the thermal layer in the diurnal and seasonal cycles are different in their nature. In the diurnal cycle the thermal structure builds up because of the direct influence of solar radiation, and its depth is limited to the effective absorption of short-wave radiation (a few meters). The thermal layer is destroyed at nighttime because of wind-driven vertical mixing. As a result of the vertical mixing, the heat absorbed during the daytime in the uppermost layer is transferred down to deeper levels, and the seasonal epilimnion (upper ~20 m) gradually builds up. In the late autumn, the seasonal epilimnion is destroyed as it becomes gravitationally unstable because of cooling and an increase of salinity, resulting in full mixing [Anati, 1997]. As shown in section 5.1, the diurnal and seasonal vertical thermal structure correlates with the surface temperature pattern: the higher the vertical temperature gradient, the higher the surface temperature heterogeneity.

5.4. Summary

[22] We used satellite and in situ data to characterize the spatial and temporal variations of the Dead Sea SST and to explore the causes for these variations. Sequences of almost continuous individual satellite images were transformed into a time series of parameters representing the spatial distribution of SST. In addition, we used in situ measured bulk SST, wind speed, solar radiation, and water temperature profiles with depth. Strong diurnal and seasonal variations of the surface and vertical temperature field are related to each other and to the forcing of wind and solar radiation. In the diurnal cycle, the temperature field is heterogeneous after noon, when radiation is high and wind speed is low and thermal layering develops. At nighttime, the homogeneous temperature field (both vertically and at the surface)

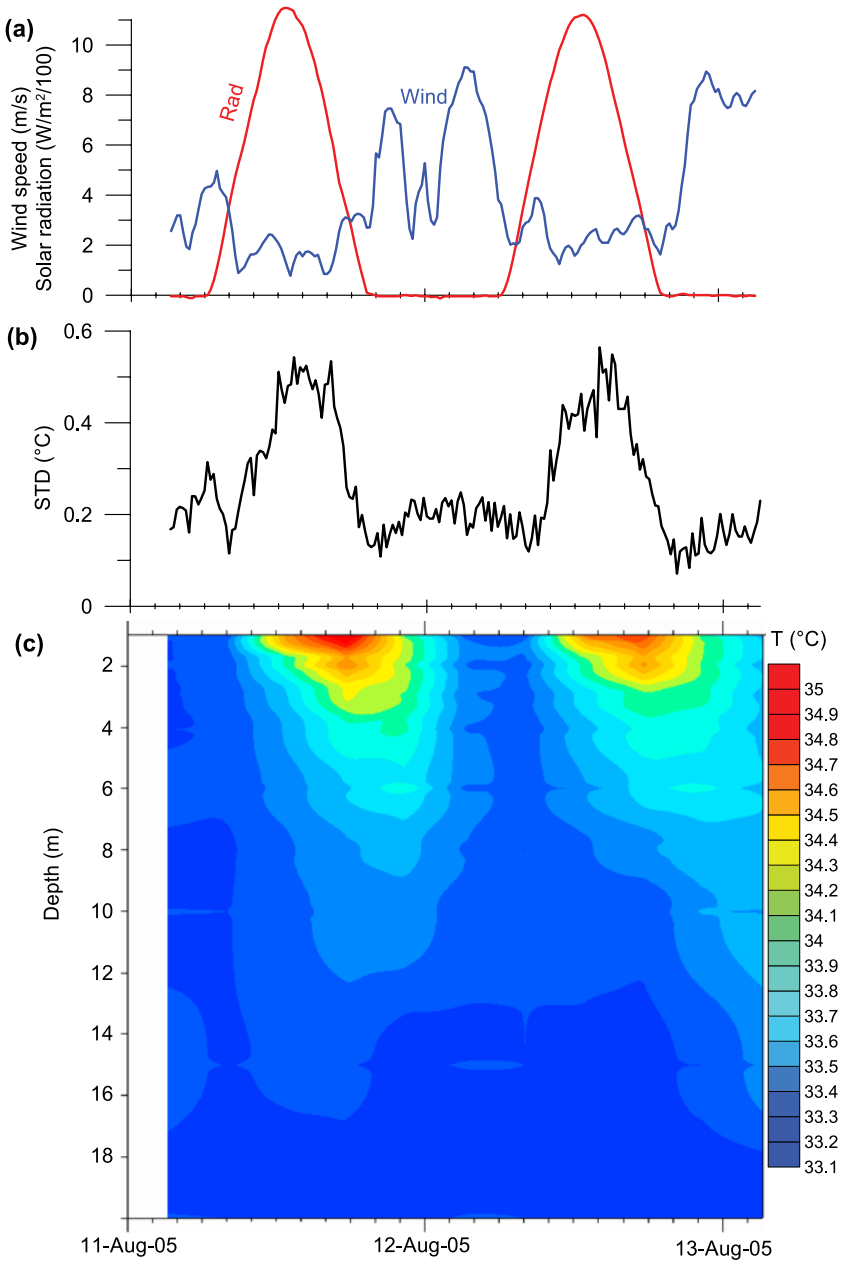

Figure 5. The diurnal thermal structure of the Dead Sea: (a) wind speed and solar radiation, (b) the standard deviation of SST (horizontal variations), and (c) the vertical temperature profile. Note that the SST variations increase (Figure 5b) as the upper water layer warms up (Figure 5c) because of the solar radiation (Figure 5a). During nighttime, SST variations drop dramatically (Figure 5b) with sunset and the onset of sea breeze (Figure 5a), which destroys the upper warm layer (Figure 5c).

is attributed to the influence of high wind speed and the resulting vertical mixing. The seasonal variations show higher surface temperature heterogeneity in the summer when radiation is high and thermal layering is strongly developed. These variations decrease toward the winter as the solar radiation decreases and the water column is vertically homogeneous.

[23] **Acknowledgments.** We thank Isaac Gertman for supplying the in situ measurements from the buoy, which enabled this research. We thank Ittai Gavrieli and Steve Brenner for fruitful discussions. Gerald Stanhill, Amit Mushkin, and Vladimir Lyakhovsky are acknowledged for their helpful comments on the manuscript. The research was supported by the Earth Science Research Administration, the Ministry of National Infrastructures (Israel), the Israel Science Foundation (grant 902/05), and the Schnitzer Foundation for Research on the Israeli Economy and Society. Two anonymous reviewers and the editor are greatly acknowledged for their constructive comments that improved the manuscript.

References

Alpert, P., and M. Rabinovich-Hadar (2003), Pre- and post-sea-breeze frontal lines—A Meso-γ-scale analysis over south Israel, J. Atmos. Sci., 60, 2994–3008, doi:10.1175/1520-0469(2003)060<2994:PAPFLM>2.0.CO;2.

Alpert, P., H. Shafir, and D. Issahary (1997), Recent changes in the climate at the Dead Sea—A preliminary study, Clim. Change, 37, 513–537, doi:10.1023/A:1005330908974.

Anati, D. A. (1997), The hydrography of a hypersaline lake, in The Dead Sea—The Lake and Its Setting, edited by T. Niemi, Z. Ben-Avraham, and J. Gat, pp. 89–103, Oxford Univ. Press, Oxford, U. K.

Barton, I. J. (2001), Interpretation of satellite-derived sea surface temperatures, Adv. Space Res., 28, 165–170, doi:10.1016/S0273-1177(01)00337-4.

Beyth, M., I. Gavrieli, D. Anati, and O. Katz (1993), Effects of the December 1991–May 1992 floods on the Dead Sea vertical structure, Isr. J. Earth Sci., 42, 45–47.

Emery, W. J., S. Castro, G. A. Wick, P. Schluessel, and C. Donlon (2001), Estimating sea surface temperature from infrared satellite and in situ temperature data, Bull. Am. Meteorol. Soc., 82, 2773–2785, doi:10.1175/1520-0477(2001)082<2773:ESSTFI>2.3.CO;2.

Gavrieli, I., and A. Oren (2004), The Dead Sea as a dying lake, in Dying and Dead Seas: Climatic Versus Anthropogenic Causes, edited by J. C. J. Nihoul, P. O. Zavialov, and P. P. Micklin, pp. 287–305, Kluwer Acad., Dordrecht, Netherlands.

Gertman, I., and A. Hecht (2002), The Dead Sea hydrography from 1992 to 2000, J. Mar. Syst., 35, 169–181, doi:10.1016/S0924-7963(02)00079-9.

Hecht, A., and I. Gertman (2003), Dead Sea meteorological climate, in Fungal Life in the Dead Sea, edited by E. Nevo, A. Oren, and S. P. Wasser, pp. 68–114, A. R. G. Ganter, Ruggell, Lichtenstein.

Ivanov, V. A., S. P. Lyubartseva, E. N. Mikhailova, N. B. Shapiro, and I. Gertman (2002), Model of the Dead Sea. Simulation of the variability of the thermohaline water structure in 1992–2000, Phys. Oceanogr., 12, 237–256, doi:10.1023/A:1021526925126.

Lensky, I. M., and D. Rosenfeld (2008), Clouds-Aerosols-Precipitation Satellite Analysis Tool (CAPSAT), Atmos. Chem. Phys., 8, 6739–6753.

Lensky, N. G., Y. Dvorkin, V. Lyakhovsky, I. Gertman, and I. Gavrieli (2005), Water, salt and energy balances of the Dead Sea, Water Resour. Res., 41, W12418, doi:10.1029/2005WR004084.

Levin, Z., H. Gershon, and E. Ganor (2005), Vertical distribution of physical and chemical properties of haze particles in the Dead Sea valley, Atmos. Environ., 39, 4937–4945, doi:10.1016/j.atmosenv.2005.04.039.

Li, X., W. Pichel, E. Maturi, P. Clemente-Colon, and J. F. Sapper (2001), Deriving the operational nonlinear multichannel sea surface temperature algorithm coefficients for NOAA-15 AVHRR/3, Int. J. Remote Sens., 22, 699–704, doi:10.1080/01431160010013793.

Neev, D., and K. O. Emery (1967), The Dead Sea depositional processes and environments of evaporites, Bull. Geol. Surv. Isr., 41, 147 pp.

Neumann, J. (1958), Tentative energy and water balances for the Dead Sea, Bull. Res. Counc. Isr., 7G, 137–163.

Schmetz, J., P. Pili, S. Tjemkes, D. Just, J. Kerkmann, S. Rota, and A. Ratier (2002), An introduction to Meteosat Second Generation (MSG), Bull. Am. Meteorol. Soc., 83, 977–992, doi:10.1175/1520-0477(2002)083<0977:AITMSG>2.3.CO;2.

Stanhill, G. (1985), An updated energy balance estimate of evaporation from the Dead Sea, Isr. Meteorol. Resour. Pap., vol. 3, pp. 98–116, Isr. Meteorol. Serv., Bet Dagan, Israel.

Stanhill, G. (1990), Changes in the surface temperature of the Dead Sea and its heat storage, Int. J. Climatol., 10, 519–536, doi:10.1002/joc.3370100508.

Steinhorn, I., and J. R. Gat (1983), The Dead Sea, Sci. Am., 249(4), 102–109.

Steissberg, T. E., S. J. Hook, and S. G. Schladow (2005), Characterizing partial upwellings and surface circulation at Lake Tahoe, California-Nevada, USA with thermal infrared images, Remote Sens. Environ., 99, 2–15.

Thiessen, A. H. (1911), Precipitation averages for large areas, Mon. Weather Rev., 39(7), 1082–1084.

Wick, G. A., W. J. Emery, L. H. Kantha, and P. Schlussel (1996), The behavior of the bulk-skin temperature difference under varying wind speed and heat flux, J. Phys. Oceanogr., 26, 1969–1988, doi:10.1175/1520-0485(1996)026<1969:TBOTBS>2.0.CO;2.

I. M. Lensky, R. Nehorai, and S. Shiff, Department of Geography and Environment, Bar-Ilan University, Ramat-Gan 52900, Israel. (roniqq@gmail.com)

N. G. Lensky, Geological Survey of Israel, 30 Malkhe Israel Street, Jerusalem 95501, Israel.